The multiple role of acoustic cavitations: Hydrogen production and Water treatment

Nassim Kerabchi[a]*, SlimaneMerouani[a,b], OualidHamdaoui[a]

[a] Laboratory of Environmental Engineering, Department of Process Engineering, Faculty of Engineering, Badji Mokhtar – Annaba University, P.O. Box 12, 23000 Annaba, Algeria

[b] Laboratory of Environmental Process Engineering, Faculty of Process Engineering, University of Constantine 3, 25000 Constantine, Algeria

* E-mail: kerabchi_nassim@yahoo.fr

Abstract

In the field of water treatment, the destruction of organic compounds that cannot be degraded by conventional means is a target of fundamental and applied investigations. The process based on the phenomena induced by ultrasonic cavitation has shown a potential in this regard as demonstrated by the remediation of water contaminated by organic pollutants. The chemical effects of ultrasound are due to the phenomenon of cavitation, which is the nucleation, growth and implosive collapse of bubbles in a liquid. In water, the implosion of cavitation bubbles is high-energy processes that lead to thermal reactions and to the homolysis of water and dioxygen. The scission of H_2O and O_2 in the cavities leads to the production of radical species ($HO^\bullet$, $H^\bullet$, $HOO^\bullet$) which are capable of decomposing organic matter. Hydrogen was also produced during the bubble collpape. Several indirect chemical methods such as KI oxidation, Frick reaction and H_2O_2 quantification were used to detect the production of these reactive moieties in sonochemistry. In this work, based on theoretical model of acoustic cavitation, the production of free radicals as well as hydrogen from one acoustic bubble was predicted. The influence of several sonochemical parameters, such as frequency of ultrasound, acoustic intensity and liquid temperature, on the production rate of hydroxyl radical ($HO^\bullet$) and H_2 was clarified. The obtained results showed that $HO^\bullet$ and H_2 are the main species generated during the bubble collapse. The production rate of both $HO^\bullet$ and H_2 increased with increasing acoustic intensity and decreased with increasing frequency and liquid temperature.

I. Introduction:

When an ultrasonic wave propagates through a liquid, the local pressure varies

with time and space. If a bubble is present in the liquid, its radius will expand and con-tract in response to these pressure changes. For low amplitude pressure excursions, these oscillations are sinusoidal and may last for many acoustic cycles, a phenomenon called stable cavitation. Under certain conditions, however, these oscillations may become unstable leading to the rapid collapse of a bubble during a single acoustic half-cycle. This phenomenon is called transient cavitation. High temperatures and pressures are generated within the bubble during its final stage of collapse that is thought to produce hydrogen atoms and hydroxyl radicals in aqueous solutions. Some investigators feel that temperatures sufficient to generate free radicals are sometimes produced for stable cavitation as well [1]. In this work, we extended the early model to clarify, for the first time, the effect of the operational parameters on the ultrasonic production of (HO$^\bullet$) in microscopic and macroscopic scale (the bubble and the solution, respectively). The computer simulations have been carried out for a wide range of operating parameters including frequency of ultrasound (20-1100 kHz), acoustic power (0.5-1 W cm^{-2}), and liquid temperature (20-50°C).

2. Model and computational methods:

2.1. Bubble dynamics model

The theoretical model used in the present computational study have been fully described in refs.[2, 3]. It combines the dynamic of single bubble in acoustic field with chemical kinetics consisting of a series of chemical reactions occurring in the bubble at the collapse phase. The following is a brief description of the model. A gas and vapor filled spherical bubble isolated in water oscillates under the action of a sinusoidal sound wave. The temperature and pressure in the bubble are assumed spatially uniform and the gas content of the bubble behaves as an ideal gas [4].The radial dynamics of the bubble is described by the Keller-Miksis equation that includes first order terms in the Mach number M ¼ $\dot{R}$/c [5,6]:

$$\left(1-\frac{\dot{R}}{c}\right)R\ddot{R}+\frac{3}{2}\left(1-\frac{\dot{R}}{3c}\right)\dot{R}^2 = \frac{1}{\rho_L}\left(1+\frac{\dot{R}}{c}+\frac{R}{c}\frac{d}{dt}\right)\left[p_B - P(t)\right]$$

$$P_B = p - \frac{2\sigma}{R} - 4\mu\frac{\dot{R}}{R}$$

$$P(t) = P_\infty - P_A \sin(2\pi ft) \qquad (3)$$

2.2 Chemical kinetics model:

A kinetics mechanism consisting in 25 chemical reactions and their backwards reactions (Table 1) is taken into account involving AR, O2, H2O, OH, H, O, HO2, H2 and H2O2 species. The scheme in Table 1 has been partially validated from hydrogen flame studies [7] as well as shock-tube and reactor-type experiments [8].

Rate expressions for the chemical reactions consider elementary reversible reactions involving K chemical species, which can be represented in the general form as

$$\sum_{k=1}^{K} \upsilon'_{ki} X_k \leftrightarrow \sum_{k=1}^{K} \upsilon''_{ki} X_k$$
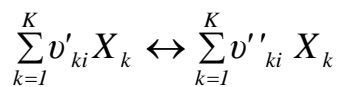
in which − in the stoichiometric coefficients of the itch reaction and X_k is the chemical symbol for the kth species. The superscript ' indicates forward stoichiometric coefficients, while " indicates reverse stoichiometric coefficients. The production rate of the kth species can be written as a summation of the rate of the variables for all reactions involving the kth species:

$$\dot{w}_k = \frac{d[X_K]}{dt} = \sum_{i=1}^{I} (\upsilon''_{ki} - \upsilon'_{ki}) r_i$$

$$r_i = k_{f_i} \prod_{k=1}^{K} [X_k]^{\upsilon'_{ki}} - k_{r_i} \prod_{k=1}^{K} [X_k]^{\upsilon''_{ki}}$$

The rate r_i for the ith reaction is given by the difference of the forward and reverse rates as

Where $[X_k]$ is the molar concentration of the kth species and k_{fi} and k_{ri} are the forward and reverse rate constants of the ith reaction, respectively. The forward and reverse rate constants for the ith reactions are assumed to have the following Arrhenius temperature dependence:

Where R_g is the universal gas constant, A_{fi} (A_{ri}) is the preexponential factor, b_{fi} (b_{ri}) is the temperature exponent and E_{fi} (E_{ri}) is the activation energy. Arrhenius parameters of each chemical reaction are listed in Table 1. In some reactions of Table 1, a third body is required for the reaction to process. When a third body is needed, the reaction rate ri of the ith reaction should be rewritten as

$$(k = 1 \ldots \ldots K) \qquad (4)$$

Table 1 : Scheme of the possible chemical reactions inside a collapsing argon bubble [9,10-14]. M is the third body. Subscript "f" denotes the forward reaction and "r" denotes the reverse reaction. A is in (cm^{3}mol^{-1}s^{-1}) for two body reaction [(cm^{6}mol^{-2}s^{-1}) for a three body reaction], and Ea is in (cal mol^{-1}).

N°	Réaction $k_{f_i} = A_{f_i} T^{b_{f_i}} \exp\left(-\dfrac{E_{a_{f_i}}}{R_g T}\right)$	A_f	b_f	E_{af}	A_r	b_r	E_{ar}
1.	$H_2O+M \leftrightarrow H^\bullet + {}^\bullet OH + M$	1.912×10^{23}	-1.83	1.185×10^5	2.2×10^{22}	-2.0	0.0
2.	$O_2+M \leftrightarrow O+O+M$	4.515×10^{17}	-0.64	1.189×10^5	6.165×10^{15}	-0.5	0.0
3.	${}^\bullet OH+M \leftrightarrow O+H^\bullet+M$	9.88×10^{17}	-0.74	1.021×10^5	4.714×10^{18}	-1.0	0.0
4.	$H^\bullet+O_2 \leftrightarrow O+{}^\bullet OH$	1.915×10^{14}	0.0	1.644×10^4	5.481×10^{11}	0.39	-2.93×10^2
5.	$H^\bullet+O_2+M \leftrightarrow HO_2^\bullet+M$	1.475×10^{12}	0.6	0.0	3.09×10^{12}	0.53	4.887×10^4
6.	$O+H_2O \leftrightarrow {}^\bullet OH+{}^\bullet OH$	2.97×10^6	2.02	1.34×10^4	1.465×10^5	2.11	-2.904×10^3
7.	$HO_2^\bullet+H^\bullet \leftrightarrow H_2+O_2$	1.66×10^{13}	0.0	8.23×10^2	3.164×10^{12}	0.35	5.551×10^4
8.	$HO_2^\bullet+H^\bullet \leftrightarrow {}^\bullet OH+{}^\bullet OH$	7.079×10^{13}	0.0	2.95×10^2	2.027×10^{10}	0.72	3.684×10^4
9.	$HO_2^\bullet+O \leftrightarrow {}^\bullet OH+O_2$	3.25×10^{13}	0.0	0.0	3.252×10^{12}	0.33	5.328×10^4
10.	$HO_2^\bullet+{}^\bullet OH \leftrightarrow H_2O+O_2$	2.89×10^{13}	0.0	-4.97×10^2	5.861×10^{13}	0.24	6.908×10^4
11.	$H_2+M \leftrightarrow H^\bullet+H^\bullet+M$	4.577×10^{19}	-1.4	1.044×10^5	1.146×10^{20}	-1.68	8.2×10^2
12.	$O+H_2 \leftrightarrow H^\bullet+{}^\bullet OH$	3.82×10^{12}	0.0	7.948×10^3	2.667×10^4	2.65	4.88×10^3
13.	${}^\bullet OH+H_2 \leftrightarrow H^\bullet+H_2O$	2.16×10^8	1.52	3.45×10^3	2.298×10^9	1.40	1.832×10^4
14.	$H_2O_2+O_2 \leftrightarrow HO_2^\bullet+HO_2^\bullet$	4.634×10^{16}	-0.35	5.067×10^4	4.2×10^{14}	0.0	1.198×10^4
15.	$H_2O_2+M \leftrightarrow {}^\bullet OH+{}^\bullet OH+M$	2.951×10^{14}	0.0	4.843×10^4	1.0×10^{14}	-0.37	0.0
16.	$H_2O_2+H^\bullet \leftrightarrow H_2O+{}^\bullet OH$	2.410×10^{13}	0.0	3.97×10^3	1.269×10^8	1.31	7.141×10^4
17.	$H_2O_2+H^\bullet \leftrightarrow H_2+HO_2^\bullet$	6.025×10^{13}	0.0	7.95×10^3	1.041×10^{11}	0.70	2.395×10^4
18.	$H_2O_2+O \leftrightarrow {}^\bullet OH+HO_2^\bullet$	9.550×10^6	2.0	3.97×10^3	8.66×10^3	2.68	1.856×10^4
19.	$H_2O_2+{}^\bullet OH \leftrightarrow H_2O+HO_2^\bullet$	1.0×10^{12}	0.0	0.0	1.838×10^{10}	0.59	3.089×10^4
20.	$O_2+O+M \leftrightarrow O_3+M$	4.1×10^{12}	0.0	-2.114×10^3	2.48×10^{14}	0.0	2.286×10^4
21.	$OH+O_2+M \leftrightarrow +O_3+H$	4.4×10^7	1.44	7.72×10^4	2.3×10^{11}	0.75	0.0
22.	$O_3.+H \leftrightarrow HO_2+O$	4.1×10^{12}	0.0	-2.114×10^3	-	-	-
23.	$O_3+O \leftrightarrow O_2+ O_2$	5.2×10^{12}	0.0	4.18×10^3	-	-	-
24.	$O_3+OH \leftrightarrow O_2+ HO_2$	7.8×10^7	0.0	1.92×10^3	-	-	-
25.	$O_3+ HO_2 \leftrightarrow O_2+ O_2+ OH$	1.0×10^{11}	0.0	2.82×10^3	-	-	-

$$k_{r_i} = A_{r_i} T^{b_{r_i}} \exp\left(-\frac{E_{a_{r_i}}}{R_g T}\right)$$

Table 2: Selected values of the ambient radius (R_0)for active bubbles as function of frequency of ultrasound, Selected   according to experimental data.

Frequency (kHz)	Ambient bubble radius, R_0 (µm)	Reference
213	3.9	[20]
355	3.2	[20]
515	3	[21]
647	2.9	[20]
875	2.7	[20]
1000	2	[20]
1100	1.4	[19]

Procedure of the numerical simulation:

The Keller Miksis equation (Eq. (1)), describing the dynamic of the bubble, is a non-linear second-order differential equation which requires an approximate numerical method for solution Eq. (1) can be reduced to a system of two differential first order equatio The system of Eqs. (8) and (9) was solved by the

$$\frac{dR}{dt} = \dot{R} \quad (8)$$

$$\frac{d\dot{R}}{dt} = \ddot{R} = \frac{\frac{1}{\rho_L}\left(1 + \frac{\dot{R}}{c} + \frac{R}{c}\frac{d}{dt}\right)[P_B - P(t)] - \frac{3}{2}\left(1 - \frac{\dot{R}}{3c}\right)\dot{R}^2}{\left(1 - \frac{\dot{R}}{c}\right)R} \quad (9)$$

fourth order Runge_Kutta method using the following initial conditions:

T= 0; R=R0 and _R = 0

The physical properties used for numerical calculations are given for water at 20 °C as .ρ_L =998.12 kg m^{-3}, s=72.45* 10^{-3}Nm^{-1}, µ= 10^{-3} kg s^{-1}m^{-1} and c= 1482ms^{-1}

The simulation of the chemical reactions in the bubble starts at the beginning of the adiabatic phase (at time corresponding to R =Rmax). The application of Eq. (4) for all species (9 species) involved in the scheme of

Table 1 gives a system of nine ordinary differential equations. For example, according to Table 1, the application of Eq. (4) to the H2O species gives:

$$w_k = \frac{1}{V}\frac{dn_{H_2O}}{dt} = -\left\{k_{f1}[H_2O][M] - k_{r1}[H^\bullet][{}^\bullet OH][M]\right\} - \left\{k_{f6}[H_2O][O] - k_{r6}[{}^\bullet OH]^2\right\} -$$
$$\left\{k_{f10}[HO_2^\bullet][{}^\bullet OH] - k_{r10}H_2O[O_2]\right\} - \left\{k_{f13}[H_2][{}^\bullet OH] - k_{r13}[H_2O][H]\right\} -$$
$$\left\{k_{f16}[H_2O_2][H^\bullet] - k_{r16}[H_2O][{}^\bullet OH]\right\} - \left\{k_{f19}[H_2O_2][{}^\bullet OH] - k_{r19}[H_2O][HO_2^\bullet]\right\}$$

When V is the volume of the bubble and nH2O is the number of moles of H2O. Using the ideal-gas law PV = n_tRT, Eq. (10) can be rewritten:

$$\frac{dn_{H_2O}}{dt} = -\frac{n_tRT}{p}\left\langle \begin{array}{c} \left\{k_{f1}[H_2O][M] - k_{r1}[H^\bullet][{}^\bullet OH][M]\right\} - \left\{k_{f6}[H_2O][O] - k_{r6}[{}^\bullet OH]^2\right\} - \\ \left\{k_{f10}[HO_2^\bullet][{}^\bullet OH] - k_{r10}H_2O[O_2]\right\} - \left\{k_{f13}[H_2][{}^\bullet OH] - k_{r13}[H_2O][H]\right\} - \\ \left\{k_{f16}[H_2O_2][H^\bullet] - k_{r16}[H_2O][{}^\bullet OH]\right\} - \left\{k_{f19}[H_2O_2][{}^\bullet OH] - k_{r19}[H_2O][HO_2^\bullet]\right\} \end{array} \right\rangle$$

(11)

where n_t is number of mole of all species present in the bubble. The input parameters for solving the system of the ordinary differential equations obtained by Eq. (4) are the composition of the bubble on water vapor and argon at time corresponding to R = Rmax, the temperature and pressure profiles in the bubble during adiabatic phase and the collapse time. These parameters are obtained by solving the dynamic Equation (Eq. (1)). As the bubble temperature increases during the adiabatic phase, the reaction system evolves and radicals start to form by thermal dissociation of H_2O in the bubble. Thus, the composition of the

bubble on all species expected to be present was determined at any temperature during the collapse period by solving the system of the ordinary differential equations obtained by Eq. (4). The system of the ordinary differential equations was solved by the finite difference method. The computer simulation of the reactions system was stopped after the end of the bubble collapse.

3. Results and discussion:

3.1. Effect of ultrasonic frequency

Practically, the most important parameter in sonolysis is the applied frequency. The effect of this parameter in the range of 20-1140 kHz on the production rate of $HO^\bullet$ and H_2 inside a collapsing Oxygen bubble is depicted in Fig. 2for an acoustic intensity of 1 W $cm^{-2}$and bulk liquid temperature

of 20 °C.. The production rate of $HO^\bullet$ is defined as its maximum amount formed at the end of the first bubble collapse multiplied by the ultrasonic frequency [22]. The ambient bubble radius (R0) employed for the numerical simulation of the bubble oscillation are selected as function of frequency (Table 1) according to the literature experimental reports. In reality, the initial size of active bubbles (R0) in cavitation field is not a single value whereas it has a range, but there is a certain size of ambient bubble radius at which a dominant number of bubbles was observed in the cavitation region. This size represents the mean ambient radius. Additionally, experiments [20, 21] showed that the range of ambient radius for active bubbles is rather narrow and it closes around the mean ambient radius As can be seen from Fig. 1, the production rate of $HO^\bullet$ and H_2decreased significantly with the increase in frequency of Ultrasound in the range 20-1100 kHz.
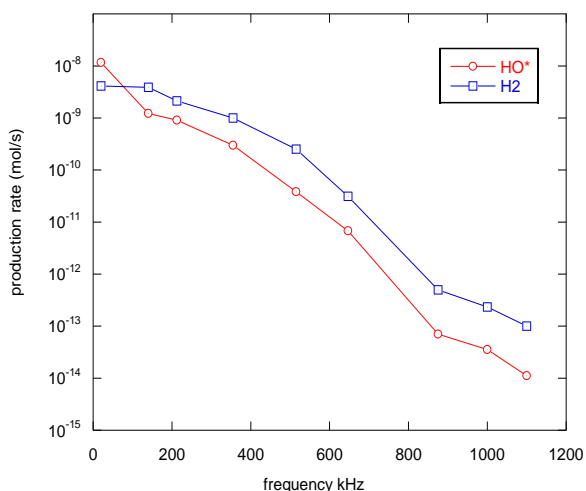
Fig. 1: Predicted production rate of HO$^\bullet$ and H$_2$ from a single bubble as function of ultrasonic frequency (conditions ambient bubble radius: Table 2; acoustic intensity: 1Wcm^{-2}; bulk liquid temperature: 20 °C). The vertical axis is in logarithmic scale.

collapse can be considered as a micro reactor within which high-temperature chemical reactions occur. The increase of both the amount of the trapped water and the collapse temperature with increasing acoustic intensity promotes the formation of free radicals since they result essentially from the dissociation of the water vapor molecules inside the bubble. Additionally, as the collapse time increases with increasing acoustic intensity, chemical reactions in the bubble at higher acoustic intensities have more time to evolve and then convert reactant molecules to free radical. Consequently, an increase in acoustic intensity will thus results in greater son chemical effects inside a bubble, leading, to higher production rate of HO$^\bullet$ and H$_2$
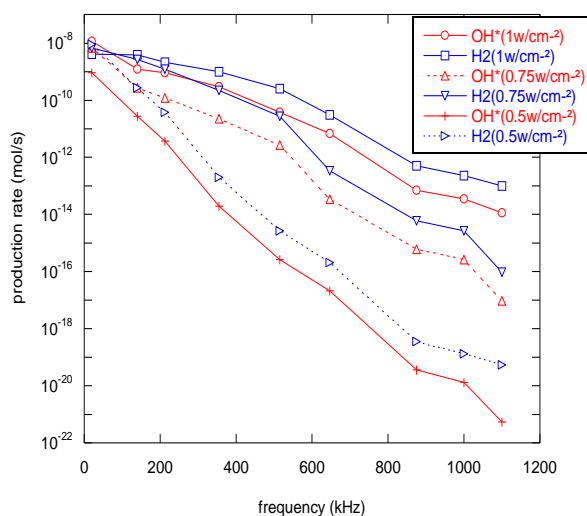
3.2. Effect of acoustic intensity

For a liquid temperature of 20°C, the effects of acoustic intensity in the interval 0.5-1Wcm^{-2} on the production rate of H$_2$ and OH inside an oxygen bubble is shown in Fig. 2for various ultrasonic frequencies (20-1100 kHz). A significant enhancement in the production rate of HO$^\bullet$ and H$_2$ was observed when the ultrasonic intensity was increased. The enhancing effect of acoustic intensity is more noticeable at high frequencies. The reason for the observed enhancement in the production rate at higher acoustic intensity may be explained as Follow. The acoustic bubble during

Fig. 2: Predicted production rate of HO$^\bullet$ from a single acoustic bubble as function of ultrasonic frequency for various acoustic intensities (conditions -ambient bubble radius: Table 2; bulk liquid temperature: 20 °C). The vertical axis is in logarithmic scale.

3.3. Effect of liquid temperature

For an acoustic intensity of 1 W cm^{-2}, computer simulations of an O$_2$-bubble oscillation and chemical reactions occurring therein were performed for diverse liquid temperature in the range 20and50 °C at various ultrasonic frequencies (20-1100 kHz). The obtained results have been shown in Fig. 3 in term of production rate of H$_2$ and OH as function of frequency for various liquid temperatures. The compression and expansion ratios of the bubble were not found to be affected by the liquid temperature variation. However, the rise in liquid temperature significantly affects the bubble temperature and the amount of the trapped water vapor as a result of the increase of liquid vapor pressure with heating. For each frequency, as the liquid temperature increases the vapor pressure increases and consequently more vapor is trapped by the collapse as. This can promote the formation of free radicals since they come from the dissociation of the water vapor molecules. But increasing liquid temperature simultaneously involves less violent collapses leading to lower internal temperature at the end of the bubble

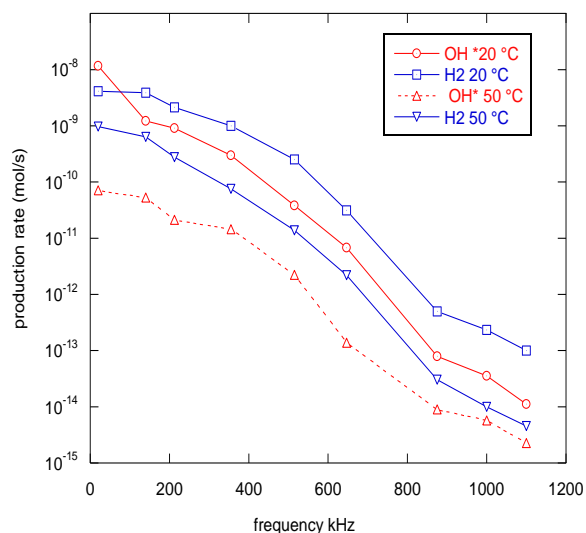collapse which reduces the decomposition of molecules into free radicals;

Fig. 3: Predicted production rate of HO$^\bullet$and H$_2$ from a single acoustic bubble as function of ultrasonic frequency for various bulk liquid temperatures (conditions _ ambient bubble radius: Table 2; acoustic intensity: 1 W cm^{-2}). The vertical axis is in logarithmic scale.

4. Conclusion

The results presented here showed the various operating conditions effect on ultrasonic production of HO$^\bullet$ and H$_2$ from the acoustic bubble has been described. The numerical simulations of the bubble oscillations and combustion reaction therein have been performed

at varied frequencies (in the range of (20-1100 kHz) for different saturating, various acoustic intensities (0.5-1W cm^{-2}) and diverse liquid temperatures (20 and 50 °C). The results of this Study is very helpful in understanding the effects of these parameters on the overall production rate of hydrogen during water sonolysis. The effect of ultrasonic frequency and Acoustic intensity on the yield of HO$^{\bullet}$ and H$_2$ was attributed to its significant impact on the cavitation process. The liquid temperature affects the bubble temperature and the bubble contents without influencing the cavitation parameters

References

[1] P. Riesz, D. Berdahl and C. L. Christman. Free Radical Generation by Ultrasound in Aqueous and Nonaqueous Solutions.Environmental Health **Perspectives Vol. 64, pp. 233-252, 1985**

[2] Merouani S, Hamdaoui O, Rezgui Y, Guemini M. Mechanism of sonochemical production of hydrogen. Int J Hydrogen Energy 2015;40:4056e64.

[3] Merouani S, Hamdaoui O, Rezgui Y, Guemini M. Theoretical procedure for the characterization of acoustic cavitation bubbles. ActaAcust United Acust 2014;100:823e33.

[4] Merouani S, Hamdaoui O, Rezgui Y, Guemini M. Theoretical estimation of the temperature and pressure within collapsing acoustical bubbles. UltrasonSonochem 2014;21:53e9.

[5] Crum LA. The polytrophic exponent of gas contained within air bubbles pulsating in a liquid. J AcoustSoc Am 1983;73:116e20.

[6] Keller JB, Kolodner II. Damping of underwater explosion bubble oscillations. J ApplPhys 1956;27:1152e61.

[7] Burdin F, Tsochatzidis NA, Guiraud P, Wilhelm AM, Delmas H. Characterisation of the acoustic cavitation cloud by two laser techniques. UltrasonSonochem 1999;6:43e51.

[8] Ohl C, Kurz T, Geisler R, Lindau O, Lauterborn W. Bubbledynamics, shock waves and sonoluminescence. Philos Trans R SocLond A 1999;357:269e94.

[9] Hart EJ, Henglein A. Sonochemistry of aqueous solutions: H2eO2 combustion in cavitation bubbles. J PhysChem1987;91:3654e6.

[10] Adewuyi YG. Sonochemistry: environmental science and engineering applications. IndEngChem Res 2001;40:4681e715.

[11] Merouani S, Hamdaoui O, Rezgui Y, Guemini M. A method for predicting the number of active bubbles in sonochemicalreactors.UltrasonSonochem 2015;22:51e8.

[12] Crum LA. The polytrophic exponent of gas contained within air bubbles pulsating in a liquid. J AcoustSoc Am 1983;73:116e20.

[13] Keller JB, Miksis MJ. Bubble oscillations of large amplitude. J AcoustSoc Am 1980;68:628e33.

[14] Colussi AJ, Weavers LK, Hoffmann MR. Chemical bubble dynamics and quantitative sonochemistry. J PhysChem A 1998;102:6927e34.

[15] Burdin F, Tsochatzidis NA, Guiraud P, Wilhelm AM, Delmas H. Characterisation of the acoustic cavitation cloud by two laser techniques. UltrasonSonochem 1999;6:43e51.

[16] Tsochatzidis NA, Guiraud P, Wilhelm A, Delmas H. Determination of velocity, size and concentration ofultrasonic cavitation bubbles by the phase-Doppler technique. ChemEngSci 2001;56:1831e40.

[17] Ohl C, Kurz T, Geisler R, Lindau O, Lauterborn W. Bubble dynamics, shock waves and sonoluminescence. PhilosTransRSocLond A 1999;357:269e94.

[18] Yasui K. Influence of ultrasonic frequency on multibubblesonoluminescence. J Am ChemSoc 2002;112:1405e13.

[19] ChenW-S,MatulaTJ,CrumLA.Thedisappearance of ultrasound contrast bubbles: observations of bubble dissolution and cavitation nucleation. UltrasoundMedBiol 2002;28:793e803.

[20] Brotchie A, Grieser F, Ashokkumar M. Effect of power and frequency on bubble-size distributions in acoustic cavitation. Phys Rev Lett 2009;102:084302e4.

[21] Lee J, Ashokkumar M, Kentish S, Grieser F. Determination of the size distribution of sonoluminescence bubbles in a pulsed acoustic field. J Am ChemSoc 2005;12(7):16810e1.

[22] Yasui K, Tuziuti T, Lee J, Kozuka T, Towada A. The range of ambient radius for an active bubble in sonoluminescenceand sonochemical reactions. J ChemPhys2008;128:184705e1
Nomenclature

c: Speed of sound in the liquid medium, m s^{1}

f: Frequency of ultrasonic wave, Hz

I: Acoustic intensity of ultrasonic irradiation, W m^{-2}

p: Pressure inside a bubble, Pa

p_{max}: Maximum pressure inside a bubble, Pa

p_{∞}: Ambient static pressure, Pa

P_A: Amplitude of the acoustic pressure, Pa

Pv: Vapor pressure of water, Pa

Pg0: Initial gas pressure, Pa

R: Radius of the bubble, m

Rmax: Maximum radius of the bubble, μm

R0: Ambient bubble radius, μm

t: Time, s

T: Temperature inside a bubble, K

Tmax: Maximum temperature inside a bubble, K

T_{∞}: Bulk liquid temperature, K

σ: Surface tension of liquid water, N m^{-1}

ρ: Density of liquid water, kg m^{-3}